MIT Libraries | DSpace@MIT

MIT Open Access Articles

Sub-5 keV electron-beam lithography in hydrogen silsesquioxane resist

The MIT Faculty has made this article openly available. ***Please share*** how this access benefits you. Your story matters.

Citation: Manfrinato, Vitor R., Lin Lee Cheong, Huigao Duan, Donald Winston, Henry I. Smith, and Karl K. Berggren. “Sub-5keV Electron-Beam Lithography in Hydrogen Silsesquioxane Resist.” Microelectronic Engineering 88, no. 10 (October 2011): 3070–3074.

Published Version: http://dx.doi.org/10.1016/j.mee.2011.05.024

Publisher: Elsevier

Permanent Link: http://hdl.handle.net/1721.1/98860

Version: Author's final manuscript: final author’s manuscript post peer review, without publisher’s formatting or copy editing

Terms of use: http://creativecommons.org/licenses/by-nc-nd/4.0/

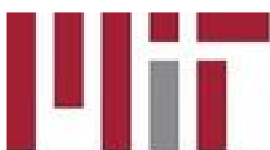

Massachusetts Institute of Technology

“NOTICE: this is the author’s version of a work that was accepted for publication in Journal of Microelectronic Engineering. Changes resulting from the publishing process, such as peer review, editing, corrections, structural formatting, and other quality control mechanisms may not be reflected in this document. Changes may have been made to this work since it was submitted for publication. A definitive version was subsequently published in Journal of Microelectronic Engineering, 88(10) 3070-3074, October 2011, DOI 10.1016/j.mee.2011.05.024”

Sub-5 keV Electron-Beam Lithography in Hydrogen Silsesquioxane Resist

Vitor R. Manfrinato, Lin Lee Cheong, Huigao Duan, Donald Winston, Henry I. Smith, Karl K. Berggren.*

Research Laboratory of Electronics, Massachusetts Institute of Technology, 77 Massachusetts Avenue, Cambridge, Massachusetts 02139

Abstract: We fabricated 9 to 30 nm half-pitch nested Ls and 13 to 15 nm half-pitch dot arrays, using 2 keV electron-beam lithography with hydrogen silsesquioxane (HSQ) as the resist. All structures with 15 nm half-pitch and above were fully resolved. We observed that the 9 and 10-nm half-pitch nested L's and the 13-nm-half-pitch dot array contained some resist residues. We obtained good agreement between experimental and Monte-Carlo-simulated point-spread functions at energies of 1.5, 2, and 3 keV. The long-range proximity effect was minimal, as indicated by simulated and patterned 30 nm holes in negative-tone resist.

Keywords: low-energy electron-beam lithography, low-voltage electron-beam lithography, hydrogen silsesquioxane, high resolution, proximity effect.

* Electronic mail: berggren@mit.edu

1. Introduction:

Electron-beam lithography (EBL) at energies 30 keV and above is a well established method of fabricating sub-20-nm-pitch structures [1, 2, 3, 4]. However, EBL at these high energies suffers from long-range proximity effects. Low-energy (sub-5 keV) EBL exhibits five key advantages over EBL at higher energies: (1) reduced dwell-time required for exposure (due to a higher resist sensitivity with only slightly reduced beam current) [5, 6, 7]; (2) lower system cost and a smaller footprint [7, 8, 9]; (3) significant reduction in long-range proximity effects [5, 7, 10]; (4) lower probability of sample damage and substrate heating [9]; and (5) more efficient delivery of energy into ultra-thin resists and self-assembled monolayers [11].

Previously, the finest pitch reported of adjacent lines fabricated at beam energies below 5 keV was 50 nm using calixarene [12], 60 nm using ZEP-7000 [12], 50 nm using poly-methyl-methacrylate (PMMA) [13], and 60 nm using hydrogen silsesquioxane (HSQ) [9,14]. This range of resolution is not sufficient for applications that require high throughput and high pattern resolution, such as photomask fabrication and multiple-electron-beam lithography for integrated circuits [7, 9]. The key challenges to achieving high resolution at low electron energies are the reduced electron range, the increased broadening of the incident beam (forward-scattering), and larger minimum spot size. To overcome these limitations, our experiments were conducted with ultra-thin (~ 15-nm-thick) HSQ in conjunction with high-contrast development (contrast value, $\gamma = 10$) [15]. Monte-Carlo models of electron scattering at sub-5 keV [16, 17] have never been tested at sub-20 nm length scales. The validity of low-energy exposure models are thus an important question in the field.

Here we report fabricating 9 to 30-nm-half-pitch nested L's structures, and 13 and 15-nm-half-pitch dot arrays at electron energy of 2 keV. The dots at the corners of the 4 µm × 4 µm arrays showed minimal deviation in diameter, indicating minimal long-range proximity effect. Monte-Carlo simulations of the point-spread function (PSF) at low electron energies are in agreement with experimental results. To demonstrate the expected reduced long-range proximity effect, we exposed a 2 µm × 2 µm area in HSQ, leaving a small central region unexposed. This type of structure would be extremely difficult to realize (even with proximity-effect correction) at higher energies.

2. Resolution Limit and Dose Requirements

The resolution of low-energy EBL is expected to be lower than that of high-energy EBL (e.g. 30 keV to 100 keV) due to increased electron scattering and generally larger spot size. In addition, the dose required to expose HSQ at low energies should also be much lower due to more efficient energy-transfer between the incoming electrons and the resist [6].

To experimentally determine the resolution limit of low-energy EBL, all samples were prepared by spin-coating HSQ (1% solids XR-1541, Dow Corning) on silicon wafers with native silicon dioxide at a spin-speed of 6.5 krpm. The resulting thickness was determined to be 15 nm using an ellipsometer. To avoid thermally-induced cross-linking of HSQ, which might lead to a loss in resolution, no pre-exposure bake was

performed [15]. Unless stated otherwise, all exposures were carried out at an electron energy of 2 keV on a Raith 150 EBL system with a thermal-field-emitter source operating at 1800 K (~ 0.5 eV energy spread), a 20 µm aperture, 50 µm field size, a working distance of 6 mm and a beam current of 64 pA. After exposure, samples were immersed in salty developer [15] for 4 min at 24°C, rinsed under deionized water for 2 min, and blown dry with nitrogen gas. The typical total processing period from spin coating to development was about 2-3 days. The fabricated structures were imaged by scanning-electron microscope (SEM) at 10 keV with ~ 6 mm working distance, and their dimensions were measured by image processing software (ImageJ).

Two designs of nested-L test structures, consisting of either five or seven single-pixel L-shaped-lines, were patterned in 15-nm-thick HSQ at half-pitches from 9 to 30 nm. Figure 1 shows nested L's at half-pitches of 9, 10, 15, 20, and 30 nm (the 15-nm-half-pitch structure was fabricated in a separate experiment). Although the 9- and 10-nm-half-pitch structures could be resolved, residual HSQ was present between the lines, and the single isolated lines washed away. On the other hand, structures patterned at 15, 20 and 30 nm half-pitches appeared to be fully developed.

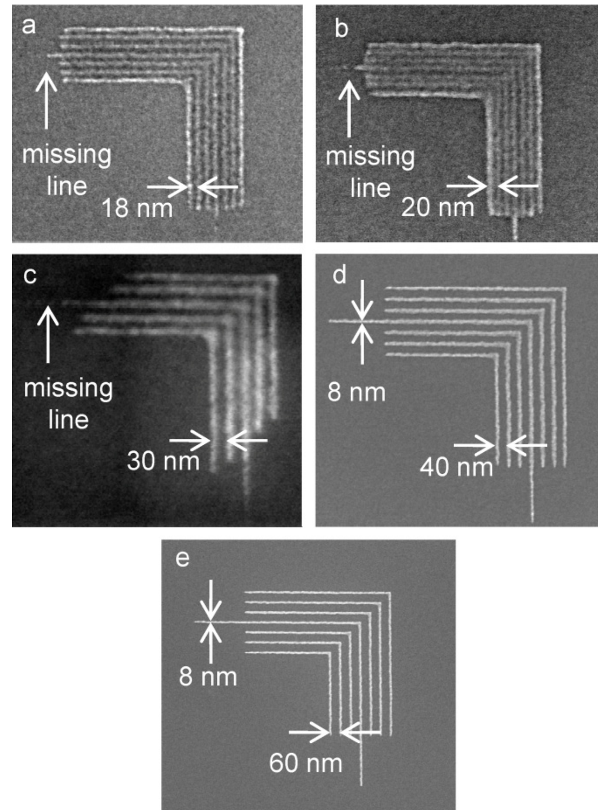

Figure 1. Scanning-electron micrographs of nested L's in 15-nm-thick HSQ exposed at 2 keV. (a) 9 nm half-pitch with a dose of 0.4 nC/cm (250 electrons/nm); (b) 10 nm half-pitch with a dose of 0.6 nC/cm (370 electrons/nm); (c) 15 nm half-pitch showing a clearly developed structure with a dose of 0.6 nC/cm (560 electrons/nm) (this experiment used cascading nested L's); (d) 20 nm half-pitch with a dose of 0.9 nC/cm (560 electrons/nm); and (e) 30 nm half-pitch with a dose of 1 nC/cm (620 electrons/nm).

As previously suggested [10], by using the ultra-thin resist we reduced the impact of forward scattered electrons, leading to higher resolution than seen previously [9, 14]. In addition, the use of HSQ with high contrast development aided in achieving higher resolution. The minimum half-pitch observed (9 nm) coincided with the electron beam spot size (9 nm), which was measured previously in [4].

To evaluate if we could maintain high resolution over large areas, we exposed 4 µm × 4 µm dot arrays on 15-nm-thick HSQ at 2 keV, with half-pitches of 15 nm and 13

nm (~ 1 Teradot/in.^{2} or ~ 0.15 Teradot/cm^2), as shown in Figures 2a and 2b, respectively. A small amount of residual HSQ was present between the 13-nm-half-pitch dots, and the dots had considerable variation in diameter. In contrast, the dots in the 15-nm-half-pitch array were uniform and without apparent residual HSQ between the dots. The dots at the corner of the array showed only minimal size deviation (~ 12 %), demonstrating that the long-range proximity effect was minimal, as expected.

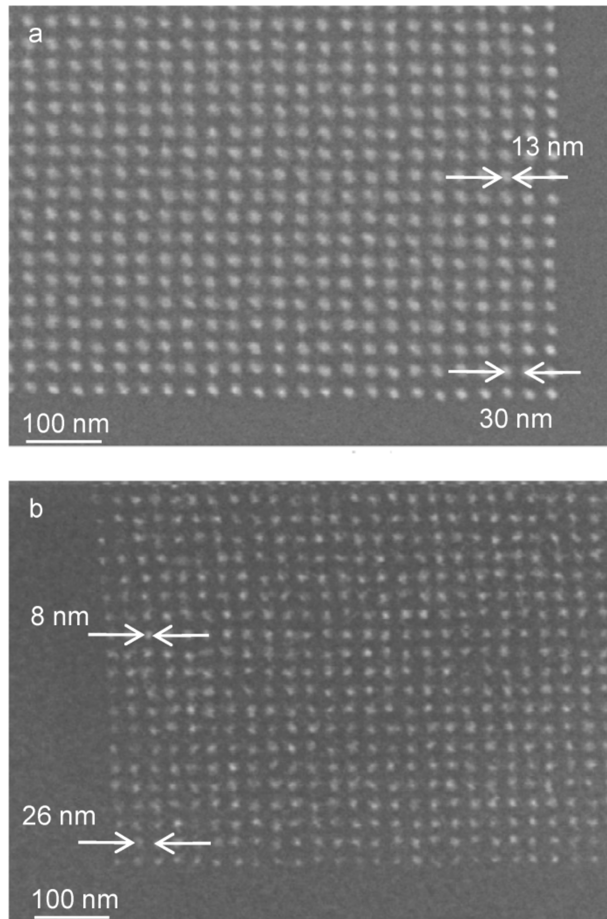

Figure 2. Scanning-electron micrographs of a corner of a 4 μm × 4 μm dot array in 15-nm-thick HSQ, exposed at 2 keV. (a) 15 nm half-pitch with a dose of 2 fC/dot (12,000 electrons/dot) and (b) 13 nm half-pitch with a dose of 1.5 fC/dot (9,300 electrons/dot). The small deviation (~ 12 %) in dot diameter between the center and the corner of the array indicated minimal proximity effect.

Patterning the same structures as shown in Figure 1 at 30 keV required 6.4 (4,000 electrons/nm) to 16 nC/cm (9,900 electrons/nm), which is roughly 16 times higher than what was required at 2 keV. Similarly, the dot array with 26-nm-pitch in Figure 2b required 1.5 fC/dot (9,300 electrons/dot) at 2 keV and 18 fC/dot (110,000 electrons/dot) at 30 keV; about 12 times higher[1]. The increased resist sensitivity at low energies may pose problems for more sensitive resists such as PMMA by causing shot noise and increased line-edge roughness [18].

3. Proximity Effect

In high-energy (e.g., 30 keV to 100 keV) EBL, a large background dose extends over several micrometers, due to back-scattered electrons. This long-range proximity effect is expected to be much less severe at low-energies due to the shorter electron range. However, this expectation has never been verified at length scales smaller than 50 nm, which is of ever-increasing importance in direct-write lithography.

We measured the point-spread function (PSF) at energies of 1.5, 2, and 3 keV. Isolated dots were patterned in 15-nm-thick HSQ with single-pixel exposures with doses ranging from 0.1 fC/dot (6×10^3 electrons) to 10^5 fC/dot (6×10^9 electrons), followed by salty development [15]. The radii of the dots were measured from SEM micrographs using image processing software (ImageJ), as described in Ref [19]. The reciprocal dot

[1] The dose comparisons made here, at 2 and 30 keV, are regarding single-pixel lines and single-dot exposures. This type of single-pixel exposures would require more dose than aerial exposures, due to the concentrated electron distribution at the center of these structures.

dose was then plotted versus the dot radius, and each PSF was normalized. Figure 3a compares the experimental PSFs we obtained with the PSF at 30 keV, determined in Ref [20] in 30-nm-thick HSQ.

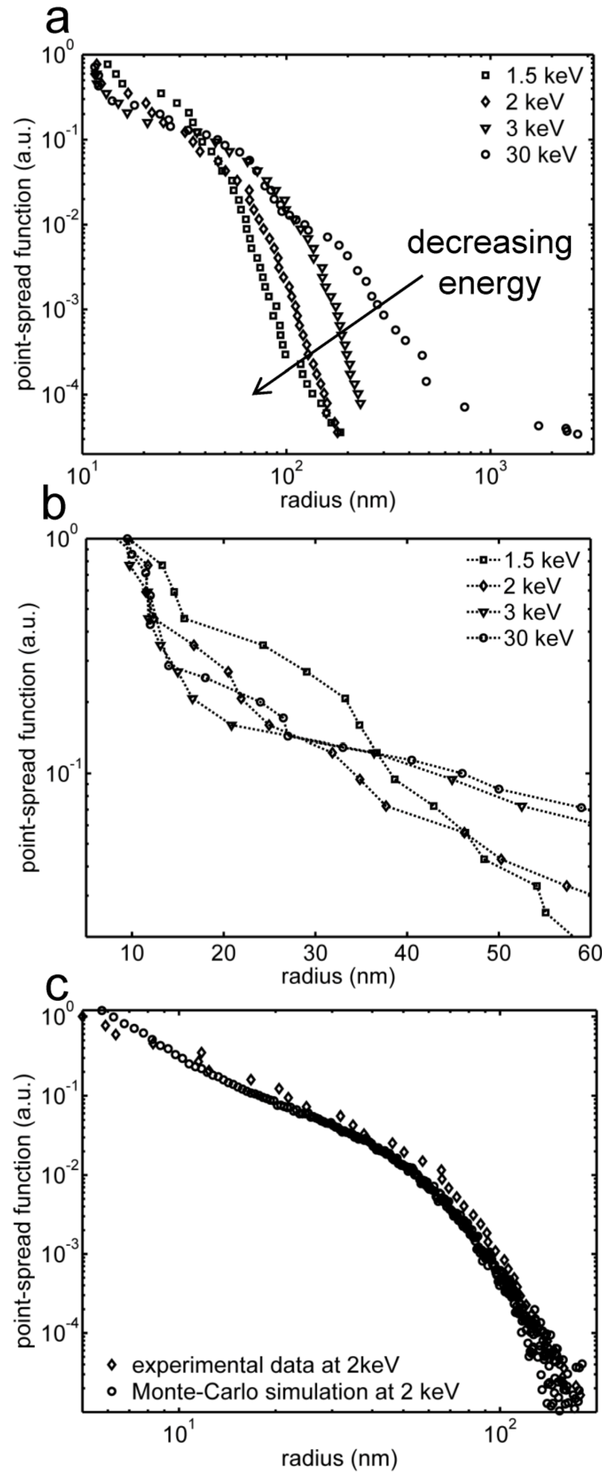

Figure 3. The point-spread function (PSF) was obtained by plotting reciprocal dot dose versus the dot radius, followed by normalization (the maximum of the PSF was set to unity). (a) PSF for 15-nm-thick HSQ at 1.5, 2, 3 keV and 30 keV for 30-nm-thick HSQ; (b) PSFs of (a) for sub-60-nm radius. The 1.5 keV PSF had widest beam spreading at sub-40-nm radius; (c) Experimental and Monte-Carlo-simulated PSFs at 2 keV, showing good agreement.

For PSF comparison in the long-range (radius bigger than 40 nm), we defined an "effective electron range", which is as a point where the dose is 10^{-5} smaller than the incident dose. At this range, the deposited dose is considered negligible for all practical purposes. As shown in the Fig. 3a, this "effective range" of the electrons at 1.5 and 2 keV is less than 200 nm. Figure 3b is a magnified view of the same PSFs at radii 60nm and below. The PSFs at 2, 3 and 30 keV are approximately the same for the short range (radius smaller than 40 nm), presumably due to the use of thin resist. Only the 1.5 keV PSF has somewhat wider beam-spreading at this short range.

A Monte-Carlo simulation based on Refs [16, 17] was conducted to determine if the measurements were in agreement with the modified Bethe energy dissipation law for low-energies. We assume that the high contrast of HSQ with salty development (contrast value, $\gamma = 10$) permits a direct comparison between the experimental and simulated PSFs. We also assume that the dose distribution of the Monte-Carlo simulation represents a close approximation to the cross-linking distribution. The experimentally determined and simulated PSFs are in good agreement for energies 1.5, 2, and 3 keV. Figure 3c is a plot of the simulated and experimental PSFs at 2 keV.

There are several possible hypotheses that could explain the small observed mismatch between simulated and experimental PSFs, seen in Figure 3c. The high but finite contrast of the salty developer causes a broadening in the PSF, as observed at large radius. Mass-transport limitation during development [21] is a possible source of experimental deviation at the sub-20 nm scale. SEM metrology is also imperfect, particularly for dots with small radius, i.e. sub-20 nm dots are expected to have proportionally larger errors in the PSF measurement.

To demonstrate the reduced scattering range at low energies, we simulated the pattern in Figure 4a and exposed the pattern shown in Figure 5a. These patterns are illustrative of and sensitive to long-range proximity effects. If the background dose in the unexposed area is less than the threshold required for HSQ to cross-link, then a hole will be present. However, if the proximity effect is substantial, the hole will be exposed by the scattered electrons.

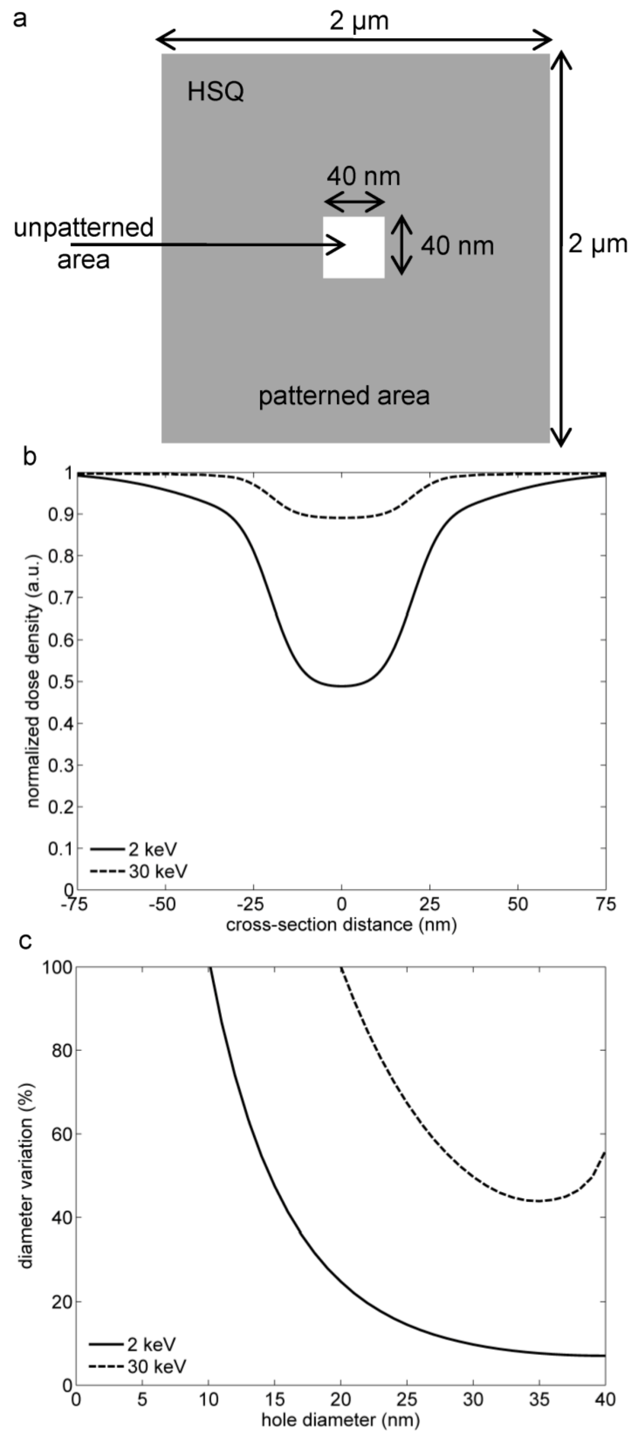

Figure 4. (a) Design of 2 μm × 2 μm patterned area with 40 nm × 40 nm unpatterned window at the center. (b) Normalized dose density (or aerial dose) calculated at the center of the unpatterned area, for low energy (2 keV) and high energy (30 keV). The exposure contrast at 2 keV is 5.5 times higher than at 30 keV.(c) Calculated process latitude (diameter variation versus hole diameter) of the pattern shown in (a),

considering a 5% dose fluctuation. The process latitude is higher and the diameter variation is lower for 2 keV than at 30 keV.

Figure 4b shows the normalized doses density (charge per unit area) calculated at the center of the pattern shown in Figure 4a for electron energies of 30 keV and 2 keV. The exposed area was divided into an address grid of 10 nm pitch (i.e., 200 × 200 address points) with 4 × 4 unexposed points at the center. For each point at position (x, y) in the structure, the distance $d(x, y; n, m)$ to every exposed point at position *(n,m)* in the array was calculated:

$$d(x, y; n, m) = \sqrt{|x - n|^2 + |y - m|^2}.$$

For this calculation we considered radially symmetric PSFs [22]:

$$PSF(r, \theta) = PSF(r)\ .$$

In order to easily manipulate the PSFs for dose distribution calculations, a fitting function was obtained for each PSF. Typical double Gaussian are used as fitting functions. However, such fitting functions are not accurate for beam energies from 2 to 30 keV. For the 2 keV PSF, we used three Gaussian functions and achieve a close fit of the PSF in the measured range. For the 30 keV PSF, we used two Gaussians plus a hyperbolic function. The physical meaning of the fitted functions is not studied in this work. Because the hyperbolic function goes to infinity for radii close to zero and we do not have any data on the 30 keV PSF for distances less than 10 nm, the hyperbolic function is only applied at 10 nm and above and goes to zero below 10 nm. The fitting parameters for the functions are provided in [23].

As described by [22], we used the abovementioned experimentally fitted PSFs to

calculate the contribution to the dose density $\delta(x,y)$ from every exposed point (with charge Q):

$$\delta(x,y) = Q\sum_{n,m} PSF\big(d(x,y;n,m)\big).$$

Exposure contrast K was used to quantify the proximity effects at the center of the pattern. K was defined as $(Dose_{\max} - Dose_{\min})/(Dose_{\max} + Dose_{\min})$, where $Dose_{\max}$ was the maximum dose in the entire pattern and $Dose_{\min}$ was the minimum dose in the unexposed central region of the pattern. As shown in Figure 4b, the background dose at 2 keV is much lower than that at 30 keV. $K = 0.06$ for 30 keV and 0.33 for 2 keV.

We also calculated the process latitude for this pattern at 2 and 30 keV, shown in Figure 4c. For holes from 0 to 40 nm diameter, a dose variation of 5% was considered. Such dose variation translates into a variation in hole diameter. Figure 4c shows a better process latitude for 2 keV exposures than at 30 keV exposures due to the reduced long-range proximity effect. For a hole with 30 nm diameter, the 2 keV exposure has ~ 10% diameter variation while the 30 keV exposure has ~ 50% diameter variation.

To experimentally confirm the dose simulation we exposed the pattern in Figure 5a. Exposures were performed using 15-nm-thick HSQ, at 2 keV and ~ 6 mm working distance with a 20 µm aperture. The samples were then developed using salty developer for 4 min at 24°C, rinsed with deionized water for 2 min, and blown dry with nitrogen gas. Figure 5b is a SEM micrograph of the fabricated pattern in the HSQ. The holes were 30 nm in diameter. A more complex pattern, spelling the letters 'EFRC', was also

fabricated (Fig. 5c) with features at the 20 nm length scale.

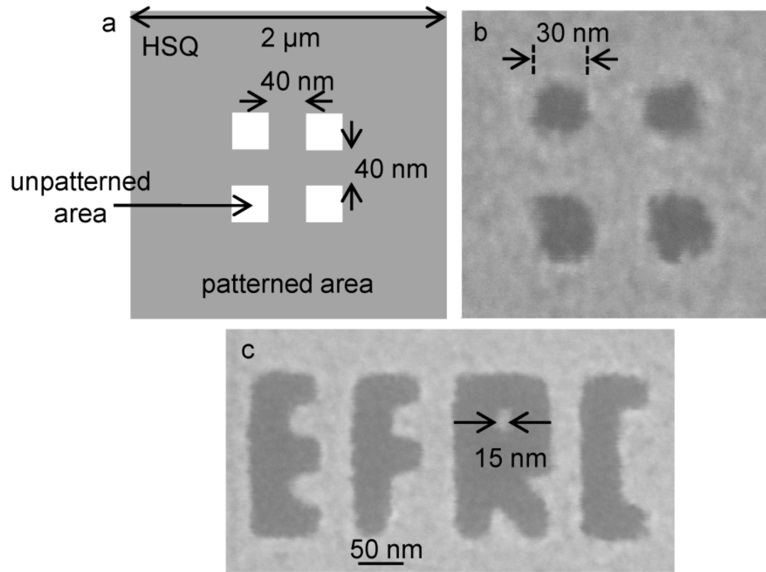

Figure 5. Holes and trenches patterned in 15-nm-thick HSQ at 2 keV. (a) Pattern consisting of 2 μm × 2 μm exposed area with 40 nm × 40 nm unexposed windows at the center. (b) Scanning-electron micrograph of close-packed 30-nm-diameter holes in HSQ, using 10 nm step size and 0.3 fC/dot (1,860 electrons/dot). (c) Scanning-electron micrograph of 'EFRC' letters with a minimum feature size of 15 nm and minimal edge roughness.

A drawback of using low-energy EBL is the difficulty in patterning thick resists. The finite penetration depth of low-energy electrons limit the maximum resist thickness possible, and forward scattering reduces resolution as the resist thickness increases [10]. The use of bi-layer or tri-layer stacks becomes necessary. Transferring high resolution patterns from resist to an underlying material is a concern due to the thinness of the electron-beam resist. Fortunately, HSQ provides better etch resistance compared to organic resists, such as poly(methylmethacrylate) (PMMA). We successfully etched 30-nm-pitch lines into 60-nm-thick XHRiC i-line anti-reflection coating polymer (Brewer Science), using 14-nm-thick HSQ as the etch mask fabricated at 2 keV [24]. The polymer

XHRiC layer was patterned using reactive-ion etching in oxygen and helium for 50s and with a radio-frequency power of 145W.

4. Conclusions

We have shown that low-energy EBL is capable of patterning with high resolution and a significantly reduced exposure dose. A resolution limit of 15-nm-half-pitch for nested L's and large-area dot array in HSQ was achieved at 2 keV. We also fabricated 9-nm-half-pitch nested L's and 13-nm-half-pitch large-area dot array, but resist residues were observed. The required dose at 2 keV was about one order of magnitude lower compared to that required at 30 keV. PSFs at low energies were experimentally determined and were in good agreement with Monte-Carlo simulations. From the experimental PSFs, the effective scattering range of electrons at energies 1.5 and 2 keV was less than 200 nm. The long-range proximity effects at sub-5-keV are much lower than at 30 keV, as demonstrated in the 'hole-in-HSQ' structures and the minimal dot diameter deviation at the corners of the large dot arrays.

The combined advantages of high resolution and reduced proximity effects make low-energy EBL an attractive alternative that may be useful for applications such as: bit-patterned media, nanoimprint molds, photomask manufacturing, and multiple-electron-beam lithography [7, 9]. With its more efficient energy transfer, low-energy EBL is also useful when patterning ultra-thin and surface-sensitive materials [11].

5. Acknowledgements

We would like to thank Jae-Byum Chang, Joseph Klingfus, Jason E. Sanabia, Euclid E. Moon, James M. Daley and Mark K. Mondol for helpful discussions. Electron-beam lithography was done in MIT's Scanning-Electron-Beam-Lithography (SEBL) shared facility in the Research Laboratory of Electronics. V. R. M. was supported as part of the Center for Excitonics, an Energy Frontier Research Center funded by the U.S. Department of Energy, Office of Science, Office of Basic Energy Sciences under Award Number DE-SC0001088. L. L. C. was supported by the National Science Foundation. H. G. D. was partially sponsored by China Scholarship Council (CSC). D. W. was supported by National Science Foundation GRFP.

6. References

[1] D. R. S. Cumming, S. Thoms, J. M. R. Weaver and S. P. Beaumont, Microelectron. Eng. **30**, 423 (1996).

[2] A. E. Grigorescu, M. C. van der Krogt, C. W. Hagen, P. Kruit, Microelectron. Eng. **84**, 822 (2007).

[3] Joel K. W. Yang, Bryan Cord, Huigao Duan, Karl K. Berggren, Joseph Klingfus, Sung-Wook Nam, Ki-Bum Kim, and Michael J. Rooks, J. Vac. Sci. Technol. B **27**, 2622 (2009).

[4] Bryan Cord, Joel Yang, Huigao Duan, David C. Joy, Joseph Klingfus, and Karl K. Berggren, J. Vac. Sci. Technol. B **27**, 2616 (2009).

[5] Y.-H. Lee, R. Browning, N. Maluf, G. Owen, and R. F. W. Pease, J. Vac. Sci. Technol. B **10**, 3094 (1992).

[6] A. Tilke, M. Vogel, F. Simmel, A. Kriele, R. H. Blick, H. Lorenz, D. A. Wharam, and J. P. Kotthaus, J. Vac. Sci. Technol. B **17**, 1594 (1999).

[7] D. Rio, C. Constancias, M. Martin, B. Icard, J. van Nieuwstadt, J. Vijverberg, and L. Pain, J. Vac. Sci.

Technol. **B** 28, C6C14 (2010).

[8] L. P. Muray, C. S. Silver, and J. P. Spallas, J. Vac. Sci. Technol. B **24**, 6, 2945 (2006).

[9] Jack J.H. Chen, S. J. Lin, T. Y. Fang, S. M. Chang, Faruk Krecinic, and Bum J. Lin, VLSI-TSA, 2009 International symposion on, 96-97 (2009).

[10] A. Olkhovets and H. G. Craighead, J. Vac. Sci. Technol. B **17**, 1366 (1999).

[11] M. J. Lercel and H. G. Craighead, A. N. Parikh, K. Seshadri, and D. L. Allara, Appl. Phys. Lett. **68**, 1504 (1996).

[12] M. Peuker, Microelectron. Eng. **53**, 337 (2000).

[13] M. A. Mohammad, T. Fito, J. Chen, S. Buswell, M. Aktary, M. Stepanova, S. K. Dew, Microelectron. Eng. **87,** 1104 (2010).

[14] A. Jamieson, C. G. Willson, Y. Hsu and A. Brodie, Proc. SPIE **4690**, 1171 (2002).

[15] J. K. W. Yang and K. K. Berggren, J. Vac. Sci. Tech. B **25**, 2025 (2007).

[16] D. C. Joy and S. Luo, *Scanning, vol.* **11**, 176 (1989).

[17] R. A. Ghanbari, Ph. D. Thesis, M.I.T. (1993) <http://hdl.handle.net/1721.1/42554>.

[18] Henry I. Smith, J. Vac. Sci. Tech B **4**, 148 (1986).

[19] R. Menon, D. Gil, and H. I. Smith, J. Opt. Soc. Am. A **23**, 567 (2006).

[20] L. Battistella, D. Winston, J. Ferrera, M. Mondol, Karl. K. Berggren, in preparation (2011).

[21] Huigao Duan, Vitor R. Manfrinato, Joel K. W. Yang, Donald Winston, Bryan M. Cord, and Karl K. Berggren, J. Vac. Sci. Tech. B **28**, C6H11 (2010).

[22] T. H. P. Chang, J. Vac. Sci. Tech. **12**, 1271 (1975).

[23] The point-spread function at 30 keV was fitted with the following model: $PSF_{30\,keV}(r) = \frac{1}{\pi(1+\eta+2\tau\ln(\beta/\alpha))}\left[\frac{1}{\alpha^2}exp\left(-\frac{r^2}{\alpha^2}\right)+\frac{\eta}{\beta^2}exp\left(-\frac{r^2}{\beta^2}\right)+\tau\frac{1}{r^2}\right]$; with fitting parameters: α = 9.5 nm; β = 3100 nm; η = 4; τ = 0.2 [20]. The hyperbolic term ($\tau\frac{1}{r^2}$) was set to zero for radii smaller than 10 nm. The point-spread function at 2 keV was fitted with the following model: $PSF_{2\,keV}(r) = \frac{1}{\pi(1+\eta+\tau)}\left[\frac{1}{\alpha^2}exp\left(-\frac{r^2}{\alpha^2}\right)+\frac{\eta}{\beta^2}exp\left(-\frac{r^2}{\beta^2}\right)+\frac{\tau}{\gamma^2}exp\left(-\frac{r^2}{\gamma^2}\right)\right]$; with fitting parameters α=10 nm; β = 40 nm; γ = 69 nm; η = 1.5; τ = 0.3.

[24] L. L. Cheong, Thesis (S.M.), M.I.T. (2010) < http://hdl.handle.net/1721.1/60159>.